http://dx.doi.org/10.5516/NET.01.2013.033

<Technical Note>

COMPUTATIONAL EFFICIENCY OF A MODIFIED SCATTERING KERNEL FOR FULL-COUPLED PHOTON-ELECTRON TRANSPORT PARALLEL COMPUTING WITH UNSTRUCTURED TETRAHEDRAL MESHES

JONG WOON KIM[1], SER GI HONG[2*], and YOUNG-OUK LEE[1]
[1]Korea Atomic Energy Research Institute
045 Daedeokdaero, Yuseong-gu, Daejeon 305-353 Korea
[2]Kyung Hee University
1732 Deogyeong-daero, Giheung-gu, Yongin-si, Gyeonggi-do, 446-701 Korea
[*]Corresponding author. E-mail : sergihong@khu.ac.kr

Received April 17, 2013
Accepted for Publication November 05, 2013

Scattering source calculations using conventional spherical harmonic expansion may require lots of computation time to treat full-coupled three-dimensional photon-electron transport in a highly anisotropic scattering medium where their scattering cross sections should be expanded with very high order (e.g., P_7 or higher) Legendre expansions.

In this paper, we introduce a modified scattering kernel approach to avoid the unnecessarily repeated calculations involved with the scattering source calculation, and used it with parallel computing to effectively reduce the computation time. Its computational efficiency was tested for three-dimensional full-coupled photon-electron transport problems using our computer program which solves the multi-group discrete ordinates transport equation by using the discontinuous finite element method with unstructured tetrahedral meshes for complicated geometrical problems. The numerical tests show that we can improve speed up to 17~42 times for the elapsed time per iteration using the modified scattering kernel, not only in the single CPU calculation but also in the parallel computing with several CPUs.

KEYWORDS : Computational Efficiency; Modified Scattering Kernel; Photon-electron Full-coupling; Three-dimensional Discrete Ordinates Method; Parallel Computing; Unstructured Tetrahedral Mesh

1. INTRODUCTION

When a photon incidents on a medium, the photon travels some considerable distance before undergoing a more catastrophic interaction leading to a partial or total transfer of the photon energy to electrons through interactions such as the photoelectric effect, Compton scattering, and pair production. These electrons will ultimately deposit their energy in the medium.

The Monte Carlo method can simulate the process above and handle a complex geometry without any assumptions or simplifications. Computer codes [1,2,3] that use the Monte Carlo method have been widely used in radiotherapy to simulate the dose distributions in multi-dimensional geometrical problems. However, fluxes and responses are calculated at pre-selected locations (tallies) and lots of computing time might be required for an accurate simulation with small statistical errors.

Compared to the Monte Carlo method, the discrete ordinates method, which is typically called the S_N method, has been widely used for neutral particle transport, but not for photon-electron full-coupled transport. Previous research [4] had been done to assess the suitability of the popular S_N neutral particle codes for coupled photon-electron calculations specific to the external beam therapy of medical physics applications. It appeared that the higher dimensional transport codes had fundamental difficulties in handling the electron transport. This is because the electron cross sections are fundamentally different from neutral particle cross sections due to the facts that electrons have highly forward peaked scattering and their inelastic scattering rapidly increases in magnitude as the energy loss approaches zero. A number of computer codes that use the S_N method require a regular mesh (rectangular, cylindrical, or spherical) to model the geometry. Use of such specific regular meshes leads to the simplest difference equations, but it may require an excessive number of mesh points to adequately model complex three-dimensional geometries.

The CEPXS [5] code provides coupled photon-electron cross sections with a multi-group Legendre form, so that conventional discrete ordinates codes and our program can solve photon-electron full-coupled transport. However, the deterministic methods using multi-group cross sections still have difficulties in treating the continuous slowing down and the forward peaking scattering of the electrons. For the geometry modeling, the use of unstructured tetrahedral meshes makes it easier to model a complicated geometry adequately.

In the discrete ordinates method for photon-electron transport, scattering sources are calculated with updated angular fluxes through the transport sweep in each iteration. If there is no up-scattering (no-coupling or partial-coupling), only the self-scattering source needs to be considered because the scattering contributions from its upper energy groups are pre-determined. However, in the photon-electron full-coupled transport case, where both up- and down-scattering exist, we should consider extra iterations to update the scattering sources contributed from all other groups in each iteration.

In conventional scattering source calculations, the scattering cross sections are expanded by using the Legendre polynomials and the angular fluxes are expanded using the spherical harmonics to deal with anisotropic scattering. This may require lots of computation time to deal with highly anisotropic cross sections, such as P_7 or above, because lots of algebraic operations for loops and functions associated with the spherical harmonics are involved. This may undermine one of the merits of deterministic methods, which is faster calculation than the Monte Carlo method.

In this paper, we introduce a modified scattering kernel approach to avoid the unnecessarily repeated calculations mentioned above. We implemented the modified scattering kernel approach and the parallel computing in our computer program which solves the multi-group discrete ordinates transport equation using the discontinuous finite element method [6] with unstructured tetrahedral meshes. The computational efficiency of the modified scattering kernel coupled with parallel computing was tested on the three-dimensional full-coupled photon-electron transport problems.

2. THEORY AND METHODOLOGY

2.1. Governing Equations

The equations we solve are the following photon-electron full-coupled multi-group transport equations:

$$\begin{aligned}&\vec{\Omega}\cdot\nabla\psi_p(\vec{r},\vec{\Omega})+\sigma_p\psi_p(\vec{r},\vec{\Omega})\\&\quad=\sum_{p'=1}^{P}\int_{4\pi}d\vec{\Omega}'\sigma_{p'\to p}(\vec{\Omega}\cdot\vec{\Omega}')\psi_{p'}(\vec{r},\vec{\Omega}')\\&\quad+\sum_{e=1}^{E}\int_{4\pi}d\vec{\Omega}'\sigma_{e\to p}(\vec{\Omega}\cdot\vec{\Omega}')\psi_e(\vec{r},\vec{\Omega}')+q_{p,ex}(\vec{r},\vec{\Omega}),\end{aligned}\tag{1a}$$

$$\begin{aligned}&\vec{\Omega}\cdot\nabla\psi_e(\vec{r},\vec{\Omega})+\sigma_e\psi_e(\vec{r},\vec{\Omega})\\&\quad=\sum_{e'=1}^{E}\int_{4\pi}d\vec{\Omega}'\sigma_{e'\to e}(\vec{\Omega}\cdot\vec{\Omega}')\psi_{e'}(\vec{r},\vec{\Omega}')\\&\quad+\sum_{p=1}^{P}\int_{4\pi}d\vec{\Omega}'\sigma_{p\to e}(\vec{\Omega}\cdot\vec{\Omega}')\psi_p(\vec{r},\vec{\Omega}')+q_{e,ex}(\vec{r},\vec{\Omega}),\end{aligned}\tag{1b}$$

where p and e are energy group indices for photons and electrons, respectively. In Eq. (1), $q_{p,ex}(\vec{r},\vec{\Omega})$ and $q_{e,ex}(\vec{r},\vec{\Omega})$ represent the external sources for photon and electron groups, respectively. $\sigma_{p'\to p}$, $\sigma_{e\to p}$, $\sigma_{e'\to e}$, and $\sigma_{p\to e}$ are the multi-group differential photon scattering cross section, electron-to-photon production cross section, electron scattering cross section, and photon-to-electron production cross section, respectively. These scattering or production cross sections are provided by the CEPXS in multi-group Legendre form.

Our program is used as a transport solver to check the computational efficiency of the modified scattering kernel coupled with parallel computing. It uses the discrete ordinates method with the latest spatial discretization scheme, which is a discontinuous finite element method with unstructured tetrahedral meshes.

2.2 Modification of the Scattering Kernel

The three-dimensional multi-group discrete ordinates equation is:

$$\begin{aligned}&\vec{\Omega}_n\cdot\nabla\psi_g(\vec{r},\vec{\Omega}_n)+\sigma_{t,g}(\vec{r})\psi_g(\vec{r},\vec{\Omega}_n)\\&\quad=q_{s,g}(\vec{r},\vec{\Omega}_n)+q_{ex,g}(\vec{r},\vec{\Omega}_n),\end{aligned}\tag{2}$$

where $q_{ex,g}(\vec{r},\vec{\Omega}_n)$ is an external source and $q_{s,g}(\vec{r},\vec{\Omega}_n)$ is a scattering source, which is expressed as:

$$q_{s,g}(\vec{r},\vec{\Omega}_n)=\sum_{g'=1}^{G}\sum_{\ell=0}^{L}\sigma_{s\ell g'\to g}(\vec{r})\sum_{m=-\ell}^{\ell}Y_{\ell m}^{*}(\vec{\Omega}_n)\,\phi_{\ell,g'}^{m}(\vec{r}).\tag{3}$$

The spherical harmonics moments of the flux in the discrete ordinates are expressed as:

$$\phi_{\ell,g'}^{m}(\vec{r})=\frac{1}{8}\sum_{n'=1}^{N(N+2)}\omega_{n'}Y_{\ell m}(\vec{\Omega}_{n'})\psi_{g'}(\vec{r},\vec{\Omega}_{n'}).\tag{4}$$

The additional theorem of the spherical harmonics states:

$$P_\ell(\vec{\Omega}_n\cdot\vec{\Omega}_{n'})=\frac{1}{2\ell+1}\sum_{m=-\ell}^{\ell}Y_{\ell m}^{*}(\vec{\Omega}_{n'})\,Y_{\ell m}(\vec{\Omega}_n),\tag{5}$$

and by using the definition of the spherical harmonics, this may be reduced to:

$$\begin{aligned}P_\ell(\vec{\Omega}_n\cdot\vec{\Omega}_{n'})&=P_\ell(\mu_n)P_\ell(\mu_{n'})\\&+2\sum_{m=1}^{\ell}\frac{(\ell-m)!}{(\ell+m)!}P_\ell^m(\mu_n)\,P_\ell^m(\mu_{n'})\cos\left[m(w_n-w_{n'})\right].\end{aligned}\tag{6}$$

Rewriting Eq. (2) with Eqs. (3)-(6), we have a conventional discrete ordinates equation in the multi-group form as:

$$\vec{\Omega}_n \cdot \nabla \psi_g(\vec{r},\vec{\Omega}_n) + \sigma_{t,g}(\vec{r})\psi_g(\vec{r},\vec{\Omega}_n) = \sum_{g'=1}^{G}\sum_{\ell=0}^{L}(2\ell+1)\sigma_{s\ell g'\to g}(\vec{r}) \times \left[\begin{array}{l} P_\ell(\mu_n)\left(\frac{1}{8}\sum_{n'=1}^{N(N+2)}\omega_{n'}P_\ell(\mu_{n'})\psi_{g'}(\vec{r},\vec{\Omega}_{n'})\right) \\ +2\sum_{m=1}^{\ell}\frac{(l-m)!}{(l+m)!}P_\ell^m(\mu_n)\cos(mw_n) \\ \times\left(\frac{1}{8}\sum_{n'=1}^{N(N+2)}\omega_{n'}P_\ell^m(\mu_{n'})\cos(mw_{n'})\psi_{g'}(\vec{r},\vec{\Omega}_{n'})\right) \\ +2\sum_{m=1}^{\ell}\frac{(l-m)!}{(l+m)!}P_\ell^m(\mu_n)\sin(mw_n) \\ \times\left(\frac{1}{8}\sum_{n'=1}^{N(N+2)}\omega_{n'}P_\ell^m(\mu_{n'})\sin(mw_{n'})\psi_{g'}(\vec{r},\vec{\Omega}_{n'})\right) \end{array}\right] + q_{ex,g}(\vec{r},\vec{\Omega}_n), \quad (7)$$

where the first term on the RHS of Eq. (7) is the scattering source term, which is scattered from other groups g' and other ordinates $\vec{\Omega}_{n'}$ to the energy group g and ordinate $\vec{\Omega}_n$.

If the anisotropy order, L, is not very high (i.e., P_3 or below), the computational burden to deal with the spherical harmonics in Eq. (7) is not much. However, in the photon-electron beam problem, electron cross sections are highly forward peaked in angle, so that it might be better to use at least P_7 or above. With a high anisotropy order in the spherical harmonics, the computational load gets heavier due to the calculations for m, ℓ, sin, cos, and $P_\ell^m(\mu_n)$ functions in the spherical harmonics in each iteration.

If there is no up-scattering, the scattering source calculation for group g in Eq. (7) is only performed on the self energy group, $g' = g$. The down-scattering source for $g' < g$ can be directly calculated with the already converged higher energy group angular fluxes. This calculation can be done on each group sequentially.

However, for the photon-electron full-coupled transport with the photon beam source, there is up-scattering (from the electron group to the photon group), so that the scattering source calculation for group g should be performed throughout all of the energy groups $g' = 1\ldots, G$.

Considering a high anisotropy order, L, and up-scattering in each iteration, the computational burden with spherical harmonics increases greatly.

To minimize this computational burden, a modified scattering kernel is introduced in the conventional discrete ordinates equation as

$$\vec{\Omega}_n \cdot \nabla \psi_g(\vec{r},\vec{\Omega}_n) + \sigma_{t,g}(\vec{r})\psi_g(\vec{r},\vec{\Omega}_n) = \sum_{g'=1}^{G}\sum_{n'=1}^{N(N+2)}\omega_{n'}\,\overline{\sigma}_{n'\to n,g'\to g}(\vec{r})\,\psi_{g'}(\vec{r},\vec{\Omega}_{n'}) + q_{ex,g}(\vec{r},\vec{\Omega}_n), \quad (8)$$

where $\overline{\sigma}_{n'\to n,\,g'\to g}(\vec{r})$ are pre-calculated group-to-group, ordinate-to-ordinate scattering cross sections and they are calculated only once in the whole calculation process.

In previous researches [7,8], the modified scattering kernel and the priority concept method to guarantee the non-negativity of the scattering cross section were introduced to deal with the non-negative scattering cross sections and showed their efficacy on the resulting flux distributions. In reference 7, the main goal was generating non-negative scattering cross sections deterministically. To do this, the authors introduced a modified scattering kernel and priority concept method. For the numerical tests, neutron and photon-electron (only partial-coupling scheme: $\gamma \to \gamma$ and $\gamma \to e$) transport were calculated in one-dimensional geometry. In reference 8, we extended the method for generating non-negative scattering cross sections to three-dimensional geometry and tested only in the neutron transport.

In this paper, we extend our program for photon-electron transport calculations in three-dimensional geometry with unstructured tetrahedral meshes. Thus, we can calculate an energy deposition profile in complicated three-dimensional geometry such as a human phantom. To solve a highly anisotropic problem effectively, we also introduced a modified scattering kernel instead of using spherical harmonics and a group-wise parallel calculation is implemented in the scattering source calculation. Compared to the previous researches, we allow negative scattering moments to deal with electron transport since the even 0^{th} moments scattering cross section of the electron group, which is generated by CEPXS, can be positive or negative in the cross section matrix. These positive or negative 0^{th} scattering moments come from the embedded continuous slowing down (CSD) cross sections in the cross section matrix.

To use the modified scattering kernel, as in Eq. (8), we need to know the group-to-group, ordinate-to-ordinate scattering cross sections, $\overline{\sigma}_{n'\to n,\,g'\to g}(\vec{r})$. Let us define the conventional scattering source for group-to-group ($g' \to g$) and ordinate-to-ordinate ($n' \to n$) as:

$$S^{SPH}_{n'\to n,g'\to g} \equiv \sum_{\ell=0}^{L}(2\ell+1)\sigma_{s\ell g'\to g}(\vec{r}) \times \left[\begin{array}{l} P_\ell(\mu_n)\left(\frac{1}{8}\omega_{n'}P_\ell(\mu_{n'})\psi_{g'}(\vec{r},\vec{\Omega}_{n'})\right) \\ +2\sum_{m=1}^{\ell}\frac{(l-m)!}{(l+m)!}P_\ell^m(\mu_n)\cos(mw_n) \\ \times\left(\frac{1}{8}\omega_{n'}P_\ell^m(\mu_{n'})\cos(mw_{n'})\psi_{g'}(\vec{r},\vec{\Omega}_{n'})\right) \\ +2\sum_{m=1}^{\ell}\frac{(l-m)!}{(l+m)!}P_\ell^m(\mu_n)\sin(mw_n) \\ \times\left(\frac{1}{8}\omega_{n'}P_\ell^m(\mu_{n'})\sin(mw_{n'})\psi_{g'}(\vec{r},\vec{\Omega}_{n'})\right) \end{array}\right]. \quad (9)$$

Also, we define the scattering source with the modified scattering kernel for group-to-group and ordinate-to-ordinate as:

$$S^{MODI}_{n'\to n,g'\to g} \equiv \omega_{n'}\,\overline{\sigma}_{n'\to n,g'\to g}(\vec{r})\,\psi_{g'}(\vec{r},\vec{\Omega}_{n'}). \quad (10)$$

The main idea of the modified scattering kernel is that we prefer to use pre-calculated group-to-group, ordinate-to-ordinate scattering cross sections which will provide the same scattering source as with the conventional one without additional calculations in the iterative calculation (directly use the angular flux without the calculations of the spherical harmonic moments).

Thus, we equate Eq. (9) to Eq. (10) as:

$$S^{MODI}_{n'\to n,g'\to g} = S^{SPH}_{n'\to n,g'\to g}. \tag{11}$$

Put Eqs. (9) and (10) into Eq. (11) and rewrite it for $\overline{\sigma}_{n'\to n,\, g'\to g}(\vec{r})$, we can then obtain:

$$\begin{aligned}\overline{\sigma}_{n'\to n,g'\to g}(\vec{r}) &= \sum_{\ell=0}^{L}(2\ell+1)\sigma_{s\ell g'\to g}(\vec{r}) \\ &\times\left[\begin{array}{l} P_\ell(\mu_n)\left(\frac{1}{8}P_\ell(\mu_{n'})\right) \\ +2\sum_{m=1}^{\ell}\frac{(l-m)!}{(l+m)!}P_\ell^m(\mu_n)\cos(mw_n) \\ \quad\times\left(\frac{1}{8}P_\ell^m(\mu_{n'})\cos(mw_{n'})\right) \\ +2\sum_{m=1}^{\ell}\frac{(l-m)!}{(l+m)!}P_\ell^m(\mu_n)\sin(mw_n) \\ \quad\times\left(\frac{1}{8}P_\ell^m(\mu_{n'})\sin(mw_{n'})\right)\end{array}\right].\end{aligned} \tag{12}$$

Eq. (12) is the final form of the group-to-group, ordinate-to-ordinate scattering cross sections, $\overline{\sigma}_{n'\to n,\, g'\to g}(\vec{r})$, and these are pre-calculated once before the whole transport calculation.

Once $\overline{\sigma}_{n'\to n,\, g'\to g}(\vec{r})$ is pre-calculated, we use the resulting cross sections in the modified scattering kernel instead of using the conventional spherical harmonics scattering kernel. By using the modified scattering kernel, we can avoid unnecessarily repeated calculations, which are affected by anisotropy order, L. In addition, high order anisotropy (P_{15} or above) is not a computational burden any more since the modified scattering kernel only considers the loop for the directional ordinates, ($n' \to n$), and energy group, ($g' \to g$).

2.3 Multi-group Legendre Photon-Electron Coupled Cross Sections

In this section, we introduce the structure of multi-group Legendre photon-electron coupled cross sections, which are generated by the CEPXS code. It will help to understand how up- and down-scattering matrix consists with, depending on the coupling schemes.

CEPXS generates the coupled electron-photon cross sections in a multi-group Legendre format. The physical models contained in CEPXS are adequate to describe the electron/photon cascade over the energy range of 100 MeV to 1.0 keV.

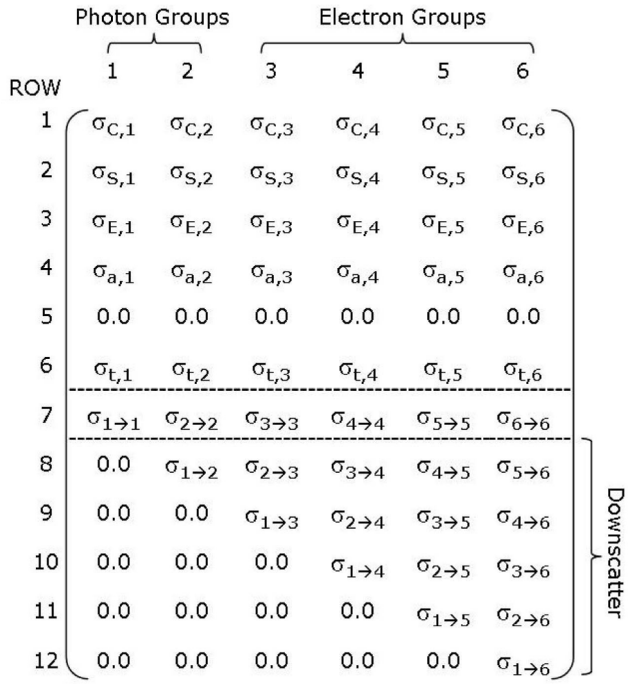

Fig. 1. Typical Global Cross Section Matrices of 0th Legendre Order (Photon-source and Partial-coupling).

To generate cross sections, an energy bound (maximum and cutoff energy), Legendre order, number of groups and type (linear or logarithmic group structure), source particle type (electron or photon source), coupling scheme (no-coupling, partial-coupling, full-coupling), and material composition are required as input parameters for the CEPXS. The coupling schemes, if the source particles are electrons, are classified into the following three categories: 1) no-coupling, electrons only, 2) partial-coupling, electrons produce photons but photons do not produce electrons, and 3) full-coupling, electrons produce photons and photons produce electrons. For the photon source, coupling schemes are the same as the electron source except that the electrons are replaced by photons, and the photons are replaced by electrons.

The resulting multi-group Legendre photon-electron coupled cross sections are given as σ_C: charged particle deposition (electrons/cm), σ_S: secondary production (particles/cm), σ_E: energy deposition (MeV/cm), σ_a: absorption (1/cm), σ_t: total (1/cm), and $\sigma_{g'\to g}$: scattering cross section (1/cm).

Figure 1 shows an example of global cross section matrices of 0th Legendre order for the partial-coupling with photon-source case.

For a partial-coupling case, we can find the solution of Eq. (7) or Eq. (8) by sweeping the angular fluxes from the 1st group to the last group in order. When we solve the 1st group, only the within group scattering ($\sigma_{1\to1}$) is considered. For the 2nd group calculation, we have two

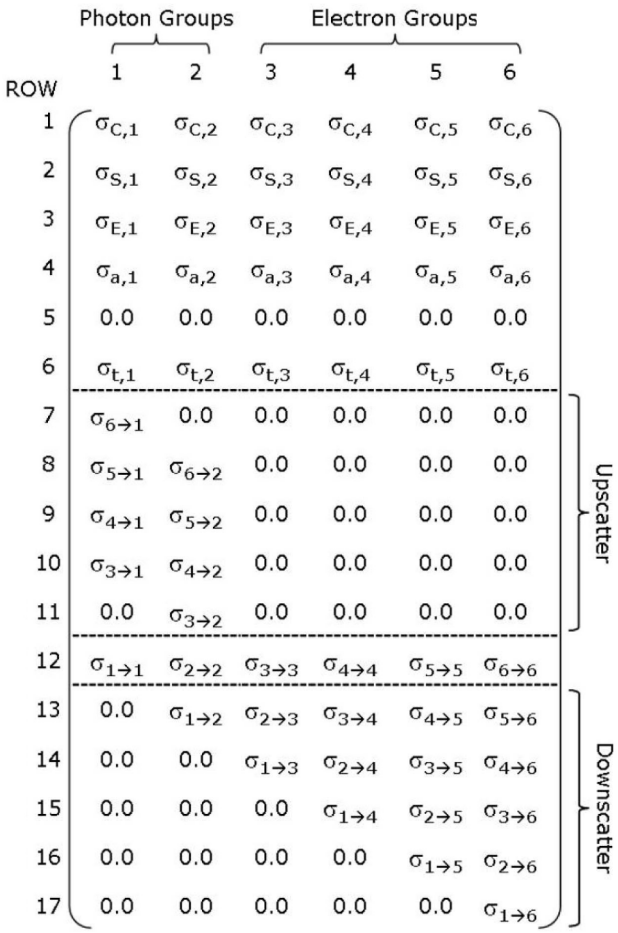

Fig. 2. Typical Global Cross Section Matrices of 0th Legendre Order (Photon-source and Full-coupling).

scattering source terms. One is the down-scattering source term from the 1st energy group ($\sigma_{1\to2}$). The other is the within group scattering source term ($\sigma_{2\to2}$). We already have the converged 1st group angular flux, so that the scattering source from the 1st group is easily calculated with a down-scattering cross section ($\sigma_{1\to2}$). The 2nd group angular flux is then calculated iteratively.

However, for the full-coupling case shown in Fig. 2, even for the 1st group, we need a scattering source from the lower groups ($\sigma_{g'\to1}$, $g' = 3, 4, 5, 6$) , which is not yet available. Because of this, we should do a transport sweep (update angular fluxes with previous scattering sources) on all energy groups ($g = 1, 2, \cdots, G$) and update the scattering sources throughout all energy groups for the next transport sweep in each iteration.

2.4 Parallel Processing

In this paper, a basic MPI parallel processing is implemented in the transport sweep and scattering source calculation. In the transport sweep, each CPU calculates angular fluxes for different ordinate directions, $\vec{\Omega}_n$. When

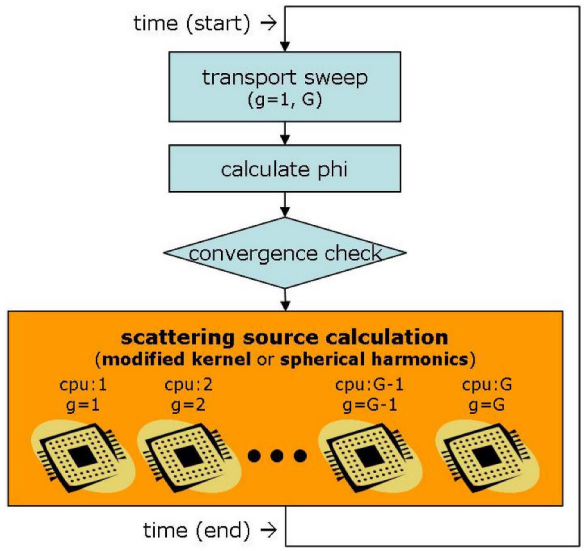

Fig. 3. Diagram to Check the Elapsed Time per Iteration for Modified Scattering Kernel and Conventional Spherical Harmonics Kernel.

the transport sweeps are done, all angular fluxes from all CPUs are gathered to calculate scalar fluxes of the energy group (g). This process is performed throughout all energy groups ($g = 1, \cdots, G$).

For the scattering source calculation, each CPU calculates the scattering source of group (g), which is scattered from other groups (g') including the ordinate-to-ordinate transfer ($n' \to n$) for the next transport sweep. In other words, group-wise parallel computing is implemented in the scattering source calculation.

In Fig. 3, the start and end time are marked, and the elapsed time per iteration is compared for two scattering kernels. All procedures are the same except the scattering source calculation part. One is with the modified scattering kernel, Eq. (8), and the other is with the conventional spherical harmonics kernel, Eq. (7).

Figure 4 shows the conceptual algorithm to calculate the scattering source, $q_{s,g}(\vec{r}, \vec{\Omega}_n)$, in Eqs. (7) and (8) where *vertex*, *n*, *elem*, and *g* are indices for vertexes of tetrahedral element, ordinate direction, tetrahedral element, and energy group. For parallel computing, the calculation of the scattering source of energy group *g*, which is the most outer loop in Fig. 4 (marked in the red bold font), is distributed to each CPU. In other words, group-wise parallel computation on energy group *g* is implemented in the scattering source calculation.

The shaded boxes in Fig. 4 show how the two kernels differ from each other in the scattering source calculation. An algorithm with the modified scattering kernel is much simpler than one with spherical harmonics, so that computational time could be reduced. In addition, high order anisotropy (P_{15} or above) is not a computational burden any more because the modified scattering kernel has nothing to do with anisotropy order, *L*.

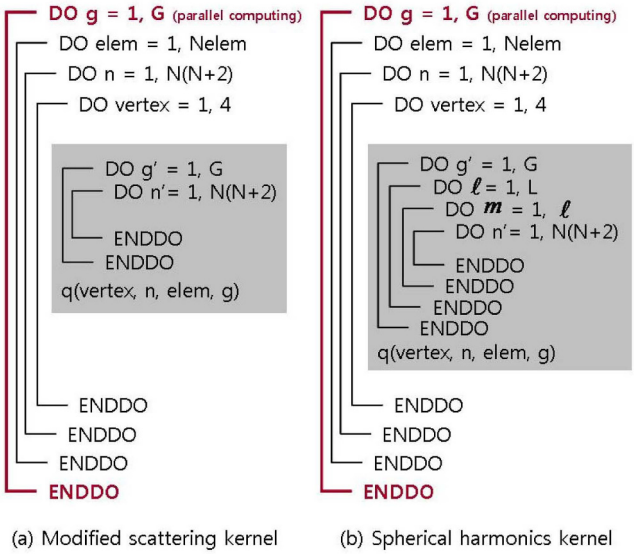

Fig. 4. Conceptual Algorithm for Calculating Scattering Source with (a) Modified Scattering Kernel and (b) Spherical Harmonics Kernel.

Comparisons of elapsed time per iteration will be shown in the next section for two test problems.

3. NUMERICAL TESTS

3.1 Simple Water Box Problem

The configuration of Test Problem I is described in Fig. 5. A 1MeV photon beam incidents on the 2cm×2cm center region (purple color) of the water slab. Cross sections are generated by CEPXS and the detailed parameters for Test Problem I are listed in Table 1.

The sectional view of the unstructured tetrahedral mesh, which was generated by Gmsh [9], for Test Problem I is shown in Fig. 6. To have a good dose profile along the centerline parallel to the Y-axis, a much finer mesh is applied in the centerline region.

The calculated three-dimensional dose profile, which is visualized by Gmsh, is shown in Fig. 7. To validate the results, the dose profile along the centerline is compared with that of MCNP5 [1]. Figure 8 shows that our calculation gives quite good agreement with the results of the MCNP5 calculation.

The elapsed times per iteration for Test Problem I are listed in Table 2. The total number of energy groups is 16, and the elapsed time per iteration is logged while varying the number of CPUs from 1 to 12. In this parallel computing, the energy group of the scattering source is distributed to the CPUs, so that the maximum parallelization can be achieved when an equal number of CPUs and energy groups are used. In other words, each CPU calculates the scattering source for one group.

With a modified scattering kernel, we can improve

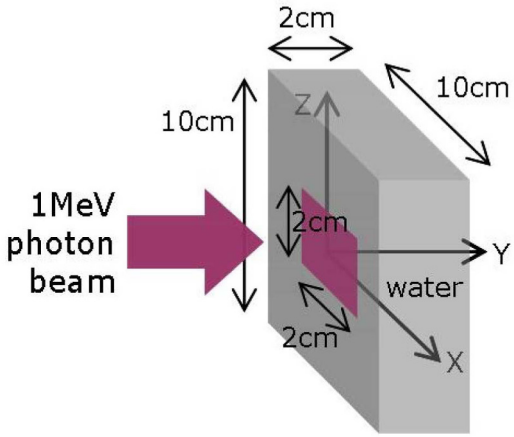

Fig. 5. The Configuration of Test Problem I (Simple Water Box Problem).

Table 1. Detailed Parameters for Test Problem I

Item	Parameters
Number of elements	19,174
Material	Water
Incident beam	1MeV Photon
Cut-off Energy	0.01 MeV
Energy group	Photon: 8 Group Electron: 8 Group
Coupling scheme	Full-coupling
Anisotropy	P_7
Angular quadrature	S_8
Mesh generation /Post-processing	Gmsh
Reference calculation	MCNP5

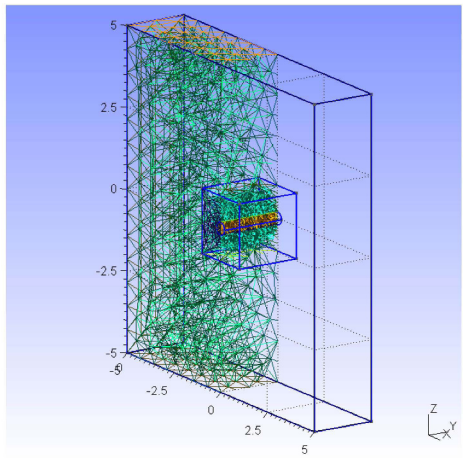

Fig. 6. A Sectional View of Unstructured Tetrahedral Mesh for Test Problem I (Simple Water Box Problem).

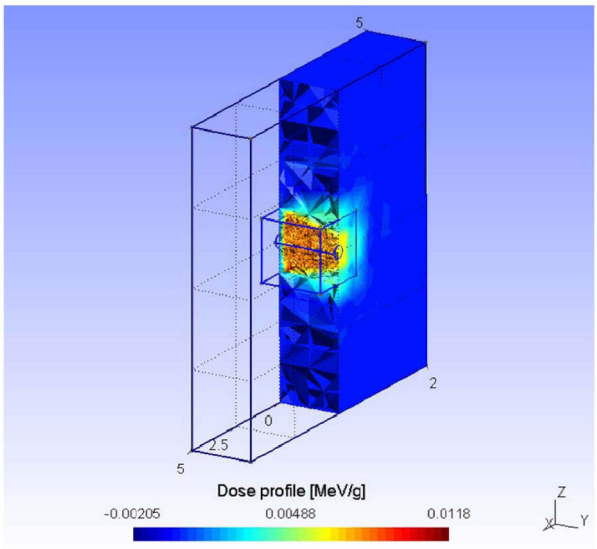

Fig. 7. A Sectional View of Dose Profile for Test Problem I (Simple Water Box Problem).

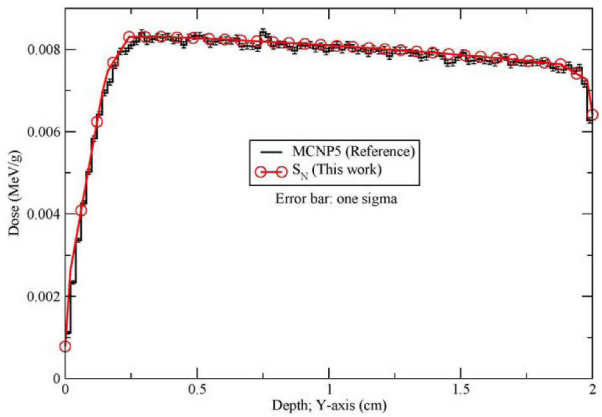

Fig. 8. A comparison of Dose Profiles along the Centerline for Test Problem I (Simple Water Box Problem).

speed by up to 35 times for an elapsed time per iteration compared to the conventional spherical harmonics kernel in the parallel computing. Even without parallel computation (i.e., with one CPU), we can have a speed increase of about 31 times.

3.2 Water Sphere in the Polyethylene Cube Problem

The configuration of Test Problem II is described in Fig. 9 where a 6MeV photon beam incidents on the left side (y=0, purple color) of a 6cm×6cm×6cm polyethylene cube. Inside of the cube, a water sphere with a 2.5cm radius is located. Cross sections are generated by CEPXS and the detailed parameters for Test Problem II are listed in Table 3.

Table 2. The Comparison of the Elapsed Times per Iteration for Two Scattering Kernels (Test Problem I)

No. of CPUs	Energy groups/CPU	Modified scattering kernel (sec/iteration)	Spherical harmonics (sec/iteration)
1	16.00	1,094	34,080
2	8.00	566	17,686
3	5.33	414	14,856
4	4.00	356	12,844
5	3.20	317	12,759
6	2.67	287	7,708
7	2.29	282	7,630
8	2.00	179	7,609
9	1.78	184	6,331
10	1.60	186	6,322
11	1.45	179	6,332
12	1.33	179	6,323

※Processor: Intel Xeon 3.4GHz CPU(6Core)×2EA, RAM: 96GB

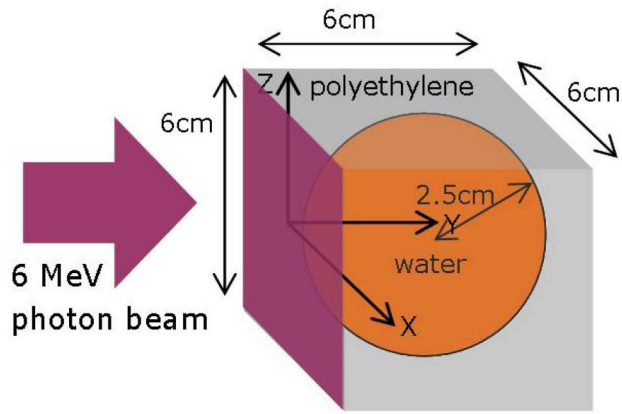

Fig. 9. A Configuration of Test Problem II (Water Sphere in the Polyethylene Cube Problem).

The sectional view of the unstructured tetrahedral mesh, which is generated by Gmsh, for Test Problem II is shown in Fig. 10.

The sectional view of three-dimensional dose distribution is shown in Fig. 11. The dose profiles along the center line, which are shown in Fig. 11, are compared with MCNP5 and shown in Fig. 12.

The horizontal sectional view of dose distribution is shown in Fig. 13. The dose profiles along the line (y=4cm and z=0, little bit shifted from the center line), which are shown in Fig. 13, are compared with MCNP5 and shown in Fig. 14.

Table 3. Detailed Parameters for Test Problem II

Item	Parameters
Number of elements	19,215
Material	Sphere: water Cube: polyethylene
Incident beam	6MeV Photon
Cut-off Energy	0.06 MeV
Energy group	Photon: 8 Group Electron: 8 Group
Coupling scheme	Full-coupling
Anisotropy	P_7
Angular quadrature	S_8
Mesh generation /Post-processing	Gmsh
Reference calculation	MCNP5

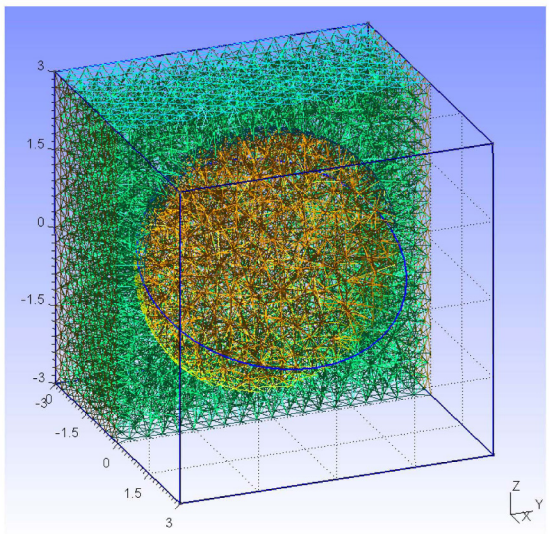

Fig. 10. A Sectional View of Unstructured Tetrahedral Mesh for Test Problem II (Water Sphere in the Polyethylene Cube Problem).

From these figures, it can be shown that the estimated dose profiles by our calculation agree well with the reference results obtained with MCNP5.

The elapsed times per iteration listed in Table 4 show a stepwise decrease as the number of CPUs is increased, and this is the same as in Test Problem I. This is because parallel computation is performed on energy group *g* mentioned in Fig. 4. In the second column of Tables 2 and 4, energy groups/CPU means how many scattering sources of energy groups each CPU should deal with. For example, in the case of 10 CPUs, the energy groups/CPU is 1.60.

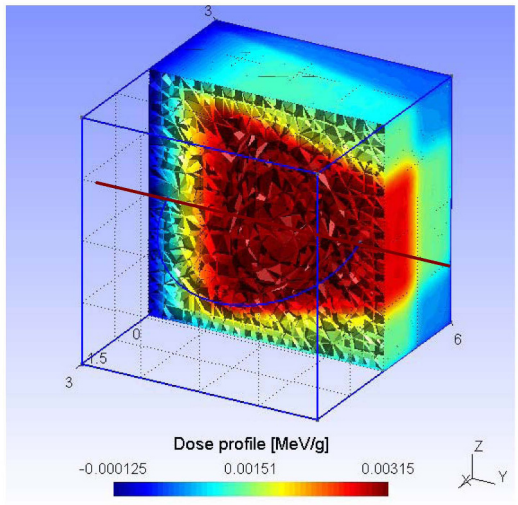

Fig. 11. A Sectional View of Dose Profile along the Center Line for Test Problem II (Water Sphere in the Polyethylene Cube Problem).

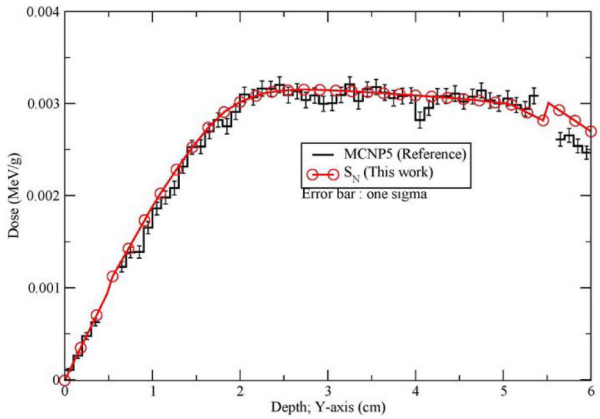

Fig. 12. A Comparison of Dose Profiles along the Centerline for Test Problem II (Water Sphere in the Polyethylene Cube Problem).

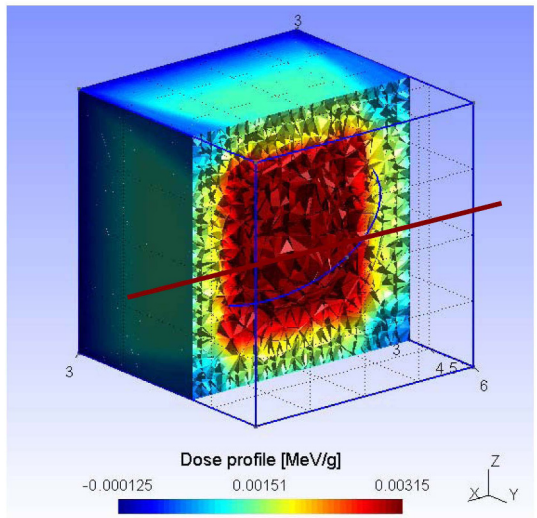

Fig. 13. A Horizontal Sectional View of Dose Profile for Test Problem II (Water Sphere in the Polyethylene Cube Problem).

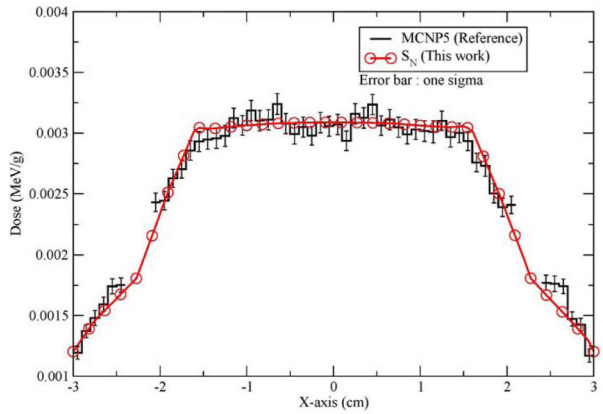

Fig. 14. A Comparison of Dose Profiles along the Horizontal Line for Test Problem II (Water Sphere in the Polyethylene Cube Problem).

Table 4. The Comparison of the Elapsed Times per Iteration for Two Scattering Kernels (Test Problem II)

No. of CPUs	Energy groups/CPU	Modified scattering kernel (sec/iteration)	Spherical harmonics (sec/iteration)
1	16.00	2,088	35,569
2	8.00	1,012	17,796
3	5.33	660	14,938
4	4.00	373	12,919
5	3.20	328	10,657
6	2.67	263	8,113
7	2.29	280	7,698
8	2.00	182	7,633
9	1.78	182	7,631
10	1.60	182	7,623
11	1.45	185	7,630
12	1.33	187	7,637

※Processor: Intel Xeon 3.4GHz CPU(6Core)×2EA, RAM: 96GB

This means that 6 CPUs calculate the scattering source for two energy groups, and 4 CPUs calculate the scattering source for one energy group since the total number of energy groups is 16. Even though 4 CPUs are done with their calculations, they should wait until the calculations of the other 6 CPUs are finished.

As shown in Tables 2 and 4, we can obtain faster calculation results with the modified scattering kernel than with the conventional spherical harmonics kernel in the iterative calculation procedure.

4. CONCLUSION

In this paper, the computational efficiency of the modified scattering kernel is analyzed on two three-dimensional photon-electron full-coupled test problems (a simple water box problem and a water sphere in the polyethylene cube problem) with our own program with implementation of the modified scattering kernel and photon-electron coupled multi-group cross sections.

The numerical tests show that we can improve speed up to 17~42 times for the elapsed time per iteration using the modified scattering kernel not only in the single CPU calculation but also in parallel computing with several CPUs.

The modified scattering kernel can be easily implemented regardless of spatial discretization schemes. In this paper, we implemented and tested it in the three-dimensional discrete ordinates transport solver, which uses the latest discontinuous finite element spatial discretization with unstructured tetrahedral elements. The numerical test also shows that our program gives very good agreement in the dose profiles with the MCNP5 reference results.

ACKNOWLEDGEMENTS

This work is supported by the Agency for Defense Development (Contract No. UC080023GD).

REFERENCES

[1] X-5 Monte Carlo team, "MCNP – A general Monte Carlo n-particle transport code, version 5, volume I, II, III," LA-CP-03-0245, Los Alamos National Laboratory (2003).

[2] I. Kawrakow, "Accurate condensed history Monte Carlo simulation of electron transport. I. EGSnrc, the new EGS4 version," *Med. Phys*., vol. 27, pp. 85-498 (2000).

[3] J.A. Halbleib, R.P. Kensek, G.D. Valdez, S.M. Seltzer, and M.J. Berger, "ITS: The integrated TIGER series of coupled electron/photon Monte Carlo transport codes – version 3.0," *IEEE. T. Nucl. Sci*., vol. 39, pp. 1025-1030 (1992).

[4] D. Ilas, M.L. Williams, D.E. Peplow, and B.L. Kirk, "Multidimensional coupled photon-electron transport simulations using neutral particle SN codes," *Computational Medical Physics Working Group Workshop II*, Gainesville, USA, (2007).

[5] L. J. Lorence Jr, J. E. Morel, and G. D. Valdez, "User's guide to CEPXS/ONEDANT: A one-dimensional coupled electron-photon discrete ordinates code package," SAND89-1661, Los Alamos National Laboratory and Sandia National Laboratory (1989).

[6] T. A. Wareing, J. M. McGhee, J. E. Morel, and S. D. Pautz, "Discontinuous finite element Sn methods on three-dimensional unstructured grids," *Nucl. Sci. Eng*., vol. 138, pp. 256-268 (2001).

[7] J. W. Kim and N. Z. Cho, "An efficient deterministic method for generating non-negative scattering cross-sections," *Ann. Nucl. Energy*, vol. 34, pp. 967-976 (2007).

[8] J. W. Kim, S. G. Hong, Y. Lee, and B. Min, "An extension of the non-negative scattering cross section generation method for a three dimensional geometry with unstructured

tetrahedral mesh," *J. Korean Phys. Soc.*, pp. 2079-2083 (2011).
[9] C. Geuzaine and J. F. Remacle, "Gmsh: a three-dimensional finite element mesh generator with built-in pre- and post-processing facilities," *Int. J. Numer. Meth. Eng.*, vol. 79[11], pp. 1309-1331 (2009).